Applied Physics B (2022) 128:16
https://doi.org/10.1007/s00340-021-07748-w

Applied Physics B
Lasers and Optics

High-power single-mode 894 nm VCSELs operating at high temperature (> 2 mW @ 365 K)

Xue li[1,2] · Yinli Zhou[1] · Xing Zhang[1] · Jianwei Zhang[1] · Yugang Zeng[1] · Yongqiang Ning[1] · Lijun Wang

Received: 3 November 2021 / Accepted: 21 December 2021 / Published online: 6 January 2022
© The Author(s) 2022

Abstract
In this study, we realize the high-power output of a single-mode 894 nm vertical-cavity surface-emitting laser (VCSEL) at high temperature. The effects of the dimensional parameters of oxide aperture and surface relief on the transverse mode and threshold gain of VCSEL were analyzed. Through collaborative optimization of the oxide aperture and relief, the VCSEL with 8 μm oxide aperture diameter and 5 μm surface relief inner diameter can operate at high temperature of 365 K with single-mode output power of 2.02 mW and side-mode suppression of 29.2 dB.

1 Introduction

Vertical-cavity surface-emitting lasers (VCSELs) are a unique type of semiconductor laser, which have the advantages of low threshold current, surface emission, high modulation speed, and small power consumption [1, 2]. Single-transverse-mode VCSELs (SM-VCSELs) are preferred optical sources for small low-power atomic sensors, including chip-scale atomic clocks, magnetometers, and gyroscopes [3]. These sensors are based on the spectral detection of alkali atoms, typically rubidium (Rb) or cesium (Cs), contained in small vapor cells. VCSELs for these atomic sensors, especially gyroscopes, must feature critical requirements [4]. When using Cs, the output power of VCSELs needs to exceed 2 mW at > 353 K, which is the operating temperature of miniature gas cells. The operating wavelength of VCSELs must be approximately 894.6 nm, corresponding to the D1 line of Cs [5]. By contrast, current commercial products can only achieve an output power of ~ 0.2 mW at 358 K, mainly for atomic clocks with lower power requirements [6]. The orthogonal polarization suppression ratios of the laser should be better than 20 dB.

✉ Yinli Zhou
zhouyinli@ciomp.ac.cn

[1] State Key Laboratory of Luminescence and Applications, Fine Mechanics and Physics, Changchun Institute of Optics, Changchun 130033, China

[2] University of Chinese Academy of Sciences, Beijing 100049, China

High-power SM-VCSELs, which can work at high temperatures, are difficult to obtain. In conventional oxide-confined VCSELs, the oxide aperture diameter is restricted to around 3 μm by the single-mode condition. Small aperture diameters suffer from large thermal resistance, and they hardly work with high power at high temperatures. The maximum output power (P_{max}) of small-aperture VCSELs at room temperature is typically less than 3 mW [7]. By detuning the gain-cavity mode, a P_{max} of ~ 1.5 mW (@ 4 mA) at 363 K is achieved in a small-aperture VCSEL [8]. Large apertures help to lower the device temperature for high output power, but can also lead to multimode operation. Therefore, various alternative approaches have been investigated to achieve high single-mode output power with aperture diameters larger than 4 μm, including photonic crystal [9] or holey-structure integrated VCSELs [10, 11], anti-resonant reflecting optical waveguide VCSELs [12], Zn-diffusion VCSELs [13], and multi-wavelength VCSELs [14].

One of the most successful techniques for SM-VCSELs is the use of a shallow surface relief etched in the top DBR of the device. This method can obtain high single-mode output power while maintaining low threshold current and high efficiency. A single-mode output power of 6.5 mW at room temperature is achieved from an 850 nm VCSEL with a shallow surface relief [15]. By employing surface grating reliefs, VCSELs with 5 μm oxide aperture show enhanced fundamental-mode emission as well as polarization stable laser oscillation. A maximum single-mode output power of 1.2 mW with side-mode suppression ratio (SMSR) of 20 dB was achieved at temperature of 353 K, and the orthogonal polarization suppression ratio is better than 20 dB [16].

In an effort to improve the output power of SM-VCSELs at high temperatures, the influence of the configuration of oxide aperture and surface relief on the mode characteristic of VCSELs are analyzed in detail in this paper. First, the basic structure of VCSELs is described, and mode analysis of the lasing region with different diameter was performed. Then, the effects of the surface relief on the threshold gain of VCSELs are calculated and the optimal relief structure parameters are determined. Finally, the photoelectric performance of VCSELs with different structure was tested for comparison. A maximum single-mode output power of 2.2 mW with SMSR of 29.2 dB was achieved at temperature of 365 K. To our knowledge, this is the best performance reported for single-mode VCSELs operating at high temperatures, which can meet the needs of higher single-mode power and high-temperature VCSELs for atomic gyroscope applications.

2 Structural design

The epitaxial structure of the VCSELs with different oxide aperture and surface relief configurations are identical. A schematic of the epitaxial and device structure is shown in Fig. 1. The N-DBR and P-DBR consist of 34.5 pairs and 22 pairs of $Al_{0.12}Ga_{0.88}As/Al_{0.9}Ga_{0.1}As$ layers, respectively. The active region is composed of three compressively strained $In_{0.06}Ga_{0.94}As$ quantum wells with a lasing wavelength of 894 nm. The oxide layer is realized by a 30 nm-thick $Al_{0.98}Ga_{0.02}As$ layer inserted between the active region and the p-DBR. The top mesa diameter is 20 μm. The diameter of the electrical injection window is 16 μm. The light emitting aperture was prepared by life-off process with diameter of 10 μm. As shown in the upper left illustration of Fig. 1, the external diameter of the circular relief is limited to 10 μm due to the light emitting aperture. The optimal inner diameter of the relief is 5 μm according to the analysis in this paper. The ring surface relief is formed by etching off the P-cap layer (23 nm thickness) and the first layer of $Al_{0.12}Ga_{0.88}As$ (40 nm thickness) of the P-DBR.

The electric field distribution and refractive index distribution along the epitaxial direction (Z direction) in the core region of the device are shown in Fig. 2a. Figure 2b shows more clearly the refractive index and electric field distribution along Z direction near the active region. In the unoxidized core region, the refractive index of $Al_{0.98}Ga_{0.02}As$ is ~ 2.98. In the oxidized cladding region, the refractive index of the oxide layer caused by Al_2O_3 decreases sharply to ~ 1.6, which lowers the effective index in the oxidized cladding region and a cylindrical waveguide is formed, having an effective index difference between core and cladding of Δ_{neff}, which is similar to the waveguide of a step-index optical fiber. The effective refractive index of the core and cladding is calculated by (1):

$$N_{clad} = \frac{\int n_{clad} * E * dz}{\int E * dz}, N_{core} = \frac{\int n_{core} * E * dz}{\int E * dz} \quad (1)$$

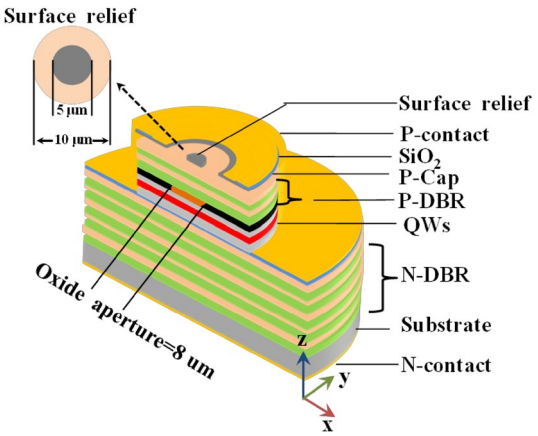

Fig. 1 Schematic of VCSELs with oxide aperture and surface relief

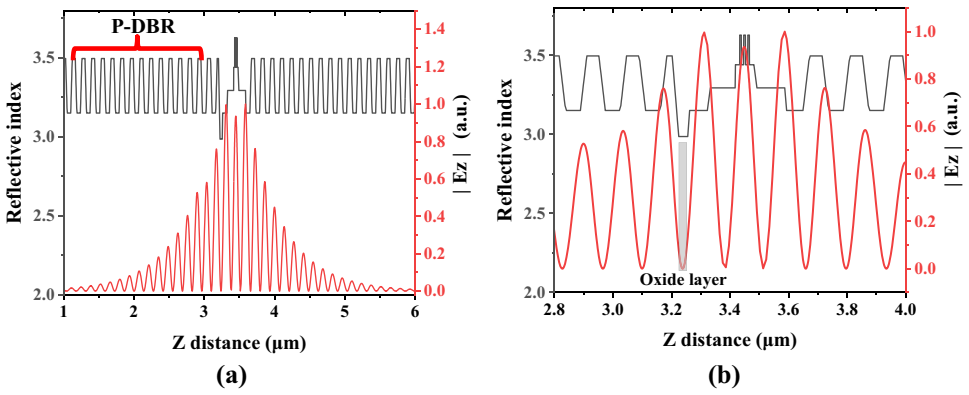

Fig. 2. **a** Electric field distribution and refractive index distribution along the epitaxial direction. **b** Refractive index and electric field distribution near the active layer

where n_{core} and n_{clad} are the material refractive indexes, E is the electric field intensity. Using Maxwell's equations and the boundary conditions at the core-cladding interface, the transverse optical modes distribution of VCSELs be calculated [17].

The oxide aperture diameter of 8 μm is adopted in this paper to realize high output power. To make the 8 μm oxidized VCSEL work in single mode, a surface relief structure was introduced by etching a circular groove on the upper surface of the device. The 1D distribution of the electric field intensities of LP_{01}, LP_{11}, and LP_{21} modes is shown in Fig. 3a. Due to the different proportion of transverse mode light distribution in the etching area, the reflectance of top DBR to different transverse mode light is different, resulting in different threshold gain (Γg_{th}) of different transverse mode. The Γg_{th} of VCSELs can be expressed as (2) [18]:

$$\Gamma g_{th} = \alpha_{in} + \alpha_{mirr}, \alpha_{mirr} = \frac{1}{L}\ln\frac{1}{\sqrt{R_t R_d}} \quad (2)$$

where Γ is the optical confinement factor, g_{th} is the threshold material gain, α_{in} is the intrinsic internal loss, α_{mirr} represents the mirror loss of the VCSELs, L is the effective cavity length of VCSELs, R_t and R_d represent the reflectivity of the top and bottom of the DBR, respectively. The reflectivity of top DBR decreases periodically with the increase of etching depth, as shown in Fig. 4b. The first extremely low reflectivity corresponds to an etching depth of 63 nm, which is equal to the sum of the thickness of the uppermost p-GaAs and p-$Al_{0.98}Ga_{0.02}As$ layers. And the etching depth of relief was adopted to 63 nm.

The effect of relief is to reduce the reflectivity of p-DBR to the light distributed in the etched region, and according to Eq. (2), the α_{mirr} of light will therefore increase. Due to the different light distribution of different transverse modes in the etched region, the α_{mirr} of different transverse modes is different, and finally affects the threshold gain. The 2-D light distribution in the XY plane of different transverse modes in the active region is calculated and shown in Fig. 3a. According to the 2-D light distribution, the light proportion of different transverse mode in the un-etched area and etched area can be calculated, respectively. Thus, the weighted reflectance R_t of p-DBR to different transverse mode light can be calculated, and the α_{mirr} of different transverse mode can be

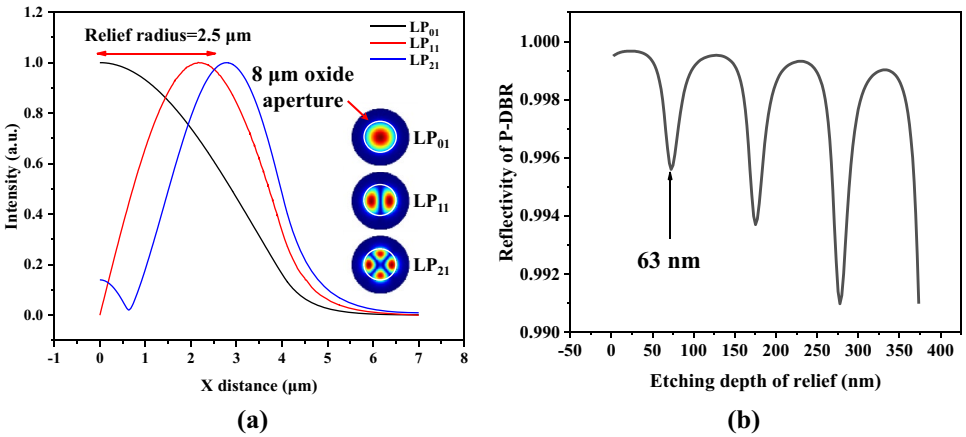

Fig. 3. **a** Distribution of the LP_{01}, LP_{11}, and LP_{21} modes along the radial direction. **b** Relationship between the Reflectivity of top DBR and etching depth of relief

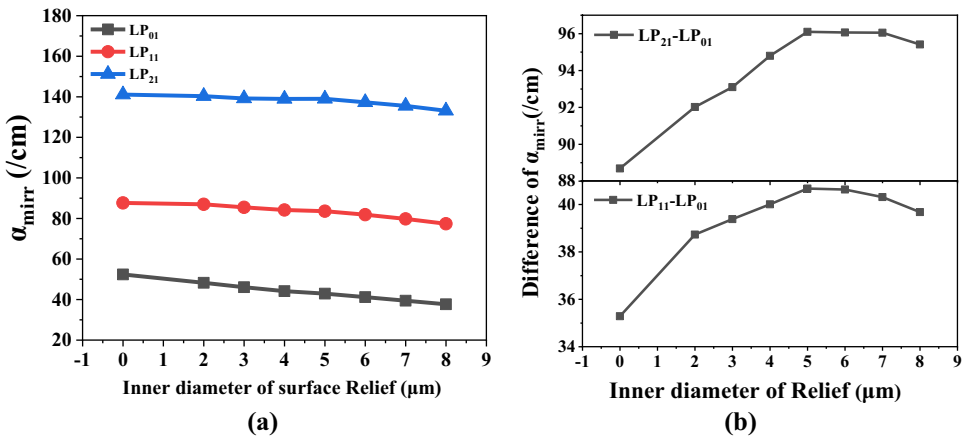

Fig. 4. **a** α_{mirr} and **b** the difference of α_{mirr} of LP_{01}, LP_{11}, and LP_{21} modes vary with the inner diameter of the surface relief of VCSELs with 8 μm oxide aperture

finally obtained. To determine the inner diameter of surface relief, we calculate the α_{mirr} of different transverse modes with different inner diameter of relief and 8 μm oxide aperture. The α_{mirr} of LP_{01}, LP_{11}, and LP_{21} modes decreases with the increase of the inner diameter of the relief, as shown in Fig. 4a. The difference of α_{mirr} is maximum when the inner diameter of the relief is 5 μm, a relief etch depth is 63 nm, as shown in Fig. 4b. Therefore, the optimal inner diameter was set at 5 μm.

3 Fabrication and experimental results

The device is fabricated through a standard process. The mesa and the surface relief are formed with inductively coupled plasma reactive ion etching. The SiO_2 insulation layer with thickness of 300 nm covers the upper surface of the entire device, and an electrical injection window is formed by etching the SiO_2 layer in the center of the mesa. The *P* metal layer was deposited on the upper surface of the device by magnetron sputtering equipment, and the lift-off process was used to prepare the light emitting aperture with a diameter of 10 μm in the center of the mesa. The oxide aperture is formed by selectively oxidizing the $Al_{0.98}Ga_{0.02}As$ layer. The SiO_2 insulating layer is deposited by plasma-enhanced chemical vapor deposition. For comparison, VCSELs with 3 μm and 8 μm oxide aperture and no relief were also prepared.

The chip was packaged in a TO56 form and installed on a commercial laser diode mount for temperature and current control. The current and temperature control accuracy are 0.001 mA and 0.01 °C, respectively. The spectral characteristics of three kinds of VCSELs at 305 and 355 K under CW condition are shown in Fig. 5. In Fig. 5a, at 305 K, the VCSEL with an 8 μm oxide aperture and 5 μm diameter relief can maintain stable single-mode operation when the current is below 7 mA. Given the decrease in carrier density in the active region at a high temperature of 355 K, the device can maintain single-mode operation at a current of 7 mA, and the SMSR is 29.92 dB. The change of wavelength with temperature is ~ 0.068 nm/K. Some unexcited modes can be seen on the shortwave side of the lasing peak because the surface relief increases the loss of the other modes of the large aperture VCSEL, making them unable to meet the threshold conditions. In Fig. 5b, the VCSEL with an 8 μm oxide aperture and no relief demonstrates a multimode simultaneous lasing at 305 K, the full width half maximum of the spectrum is larger than 1 nm. The spectrum narrowed slightly at 355 K due to the decrease in carrier density in the active region. The VCSEL with a 3 μm oxide aperture and no relief can only maintain single-mode operation when the current is less than 3 mA. At 355 K, the optical power of the device decays when the current is greater than 3 mA, as shown in Fig. 5c.

The near fields at different currents and temperatures measured using an eyepiece with a magnification of 100× are depicted in Fig. 6. To obtain clear near-field patterns and avoid detector saturation, different attenuation rates are used when testing different devices. Figure 6a depicts the near fields of VCSELs with 8 μm oxide aperture and 5 μm relief diameter. At 7 mA, a primary single-lobe spot can be seen in the near field of different temperatures, indicating the single-mode state of VCSEL. A very weak stray light distribution can be seen below the primary spot, representing the unexcited high-order mode, which is consistent with Fig. 5a. As shown in Fig. 6b, the VCSEL with 8 μm oxide aperture and no relief presents a multi-lobe near-field pattern due to multi-mode lasing. The near-field of VCSELs with 3 μm oxide aperture and no relief is shown in Fig. 6c. At 305 K, a single-lobe spot can be seen at low current, while the spot is deformed at high current due to high-order mode lasing. At 355 K, when the injection current is > 3 mA, the very high self-generated heat leads to carrier escape and the

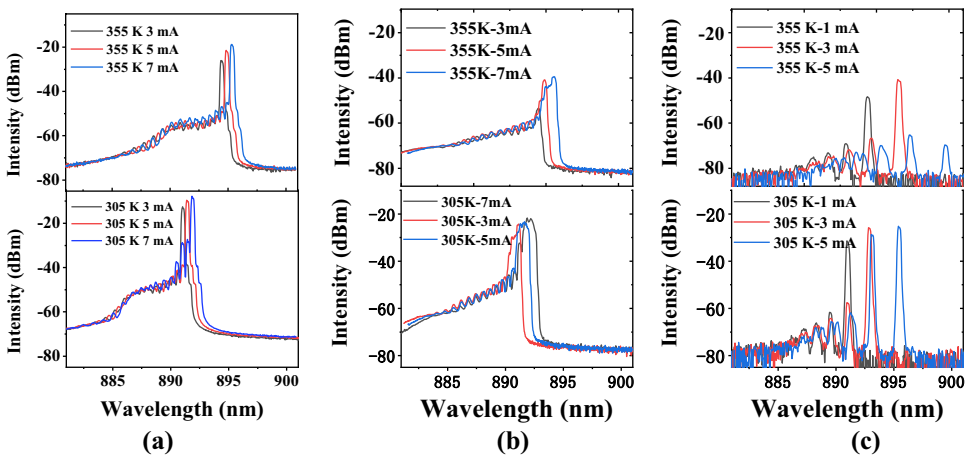

Fig. 5 Spectral characteristics of VCSELs with **a** 8 μm oxide aperture and 5 μm relief diameter; **b** 8 μm oxide aperture and no relief; **c** 3 μm oxide aperture and no relief at 305 and 355 K

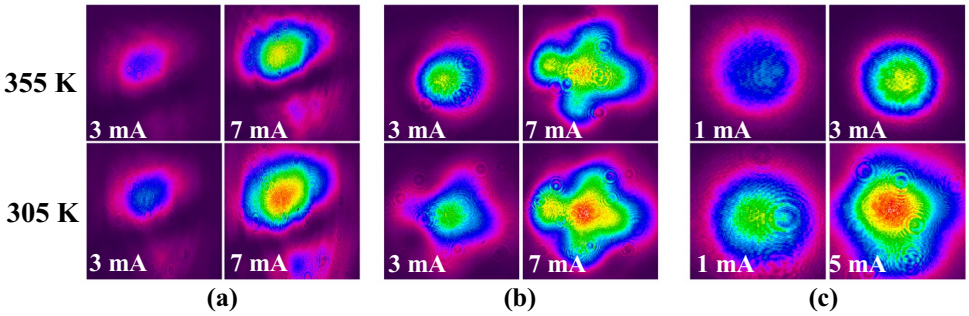

Fig. 6 Near-field patterns of VCSELs with **a** 8 μm oxide aperture and 5 μm relief diameter; **b** 8 μm oxide aperture and no relief; **c** 3 μm oxide aperture and no relief at 305 and 355 K

output power of the device decreases sharply, resulting in undetectable near-field spot.

Figure 7 depicts the power–current–voltage characteristics of the VCSEL at different temperatures under CW condition. The threshold current of the VCSEL with an 8 μm oxide aperture and 5 μm diameter relief increases from 1.06 mA at 305 K to 2.36 mA at 355 K. The maximum output power at 365 K is 2.02 mW, as shown in Fig. 7a. The 3 μm oxide aperture VCSEL has an advantage of low threshold currents (< 1 mA), as depicted in Fig. 7b. However, the output power of the device decreases rapidly with the increase in temperature and has almost no output power at 355 K. By fitting the current–voltage curves, the resistance of VCSELs with 8 μm oxide aperture is ~ 45 Ω, while that of VCSEL with 3 μm oxide aperture is ~ 190 Ω. The low resistance reduces the heat generation of the VCSEL for better high-temperature operating characteristics.

4 Conclusion

We demonstrate a high-temperature-operating 894 nm SM-VCSEL with high output power in this study. The influence of oxide aperture diameter, relief diameter and etching depth on the transverse modes of VCSELs is studied in detail by simulation and experiment. The VCSEL with 8 μm oxide aperture and 5 μm relief diameter can maintain a stable single-mode operation at high temperatures. The output power is 2.02 mW at 365 K. We believe that the high performance of the SM-VCSEL with large oxide aperture is due to the low current density in the active region and low resistance resulting in the low self-generated heat of the device. In addition, the careful optimization of the relief size enables the device to obtain the strongest higher-order mode suppression capability, which is also the reason why the device can still maintain single-mode operation at high current currents.

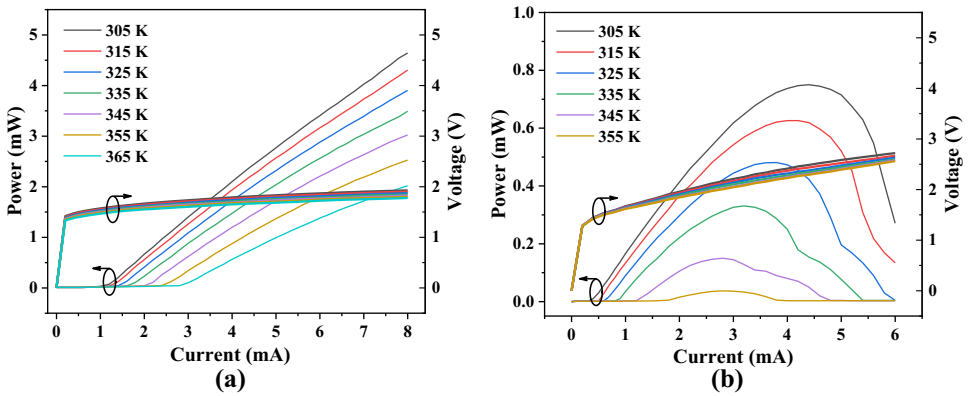

Fig. 7 Power-current–Voltage characteristics of the **a** 8 μm oxide aperture and 5 μm relied VCSELs and **b** 3 μm oxide aperture and no relief VCSELs at different temperatures

Funding National Key Research and Development Program of China (2018YFB2002400); National Natural Science Foundation of China (61804151, 52172165, 62090060, 61874117, 11774343, 61874119); Jilin Scientific and Technological Development Program (20200401006GX).

Declarations

Conflict of interest The authors declare no conflicts of interest.

Open Access This article is licensed under a Creative Commons Attribution 4.0 International License, which permits use, sharing, adaptation, distribution and reproduction in any medium or format, as long as you give appropriate credit to the original author(s) and the source, provide a link to the Creative Commons licence, and indicate if changes were made. The images or other third party material in this article are included in the article's Creative Commons licence, unless indicated otherwise in a credit line to the material. If material is not included in the article's Creative Commons licence and your intended use is not permitted by statutory regulation or exceeds the permitted use, you will need to obtain permission directly from the copyright holder. To view a copy of this licence, visit http://creativecommons.org/licenses/by/4.0/.

References

1. A. Larson, Advances in VCSELs for communication and sensing. IEEE J. Sel. Top. Quant. Electron. **17**, 1552–1567 (2011)
2. A. Kasukawa, VCSEL technology for green optical interconnects. IEEE Photonics J. **4**, 642–646 (2012)
3. J. Kitching, Chip-scale atomic devices. Appl. Phys. Rev. **5**, 031302 (2018)
4. S. Knappe, V. Gerginov, P.D.D. Schwindt, V. Shah, H.G. Robinson, L. Hollberg, J. Kitching, Atomic vapor cells for chip-scale atomic clocks with improved long-term frequency stability. Opt. Lett. **30**, 2351–2353 (2005)
5. N.A. Maleev, S.A. Blokhin, M.A. Bobrov et al., Laser source for a compact nuclear magnetic resonance gyroscope. Gyroscopy Navig. **9**, 177–182 (2018)
6. http://vixarinc.com/wp-content/uploads/2021/02/V00140.pdf
7. M. Grabherr, R. Jäger, R. Michalzik, B. Weigl, G. Reiner, K.J. Ebeling, Efficient single-mode oxide confined GaAs VCSELs emitting in the 850 nm wavelength regime. IEEE Photon. Technol. Lett. **9**, 1304–1306 (1997)
8. J.W. Zhang, X. Zhang, H.B. Zhu, J. Zhang, Y.Q. Ning, L. Qin, L.J. Wang, High-temperature operating 894.6nm-VCSELs with extremely low threshold for Cs-based chip scale atomic clocks. Opt. Express **23**, 14763–14773 (2015)
9. H. Dave, Z. Gao, S.T.M. Fryslie, B.J. Thompson, K.D. Choquette, Static and dynamic properties of coherently-coupled photonic-crystal vertical-cavity surface-emitting laser arrays. IEEE J. Sel. Top. Quant. Electron. **25**, 1–8 (2019)
10. A. Furukawa, S. Sasaki, M. Hoshi, A. Matsuzono, K. Moritoh, T. Baba, High-power single-mode vertical-cavity surface-emitting lasers with triangular holey structure. Appl. Phys. Lett. **85**, 5161–5163 (2004)
11. P. Wei, P. Guanzhong, W. Qiuhua, H. Liangchen, Z. Zhuangzhuang, X. Yiyang", 894.6nm VCSEL for Cs-Based Atomic Clocks withtriangular holey structure", 2020 3rd International Conference on Electron Device and Mechanical Engineering (ICEDME), 573–575 (2020).
12. N.N. Ledentsov, V.A. Shchukin, V.P. Kalosha, N.N. Ledentsov, J.-R. Kropp, M. Agustin, Ł Chorchos, G. Stępniak, J.P. Turkiewicz, J.-W. Shi, Anti-waveguiding vertical-cavity surface-emitting laser at 850 nm: from concept to advances in high-speed data transmission. Opt. Express **26**, 445–453 (2018)
13. J.W. Shi, Z. Khan, R.H. Horng, H.Y. Yeh, C.K. Huang, C.Y. Liu, J.C. Shi, Y.H. Chang, J.L. Yen, J.K. Sheu, High-power and single-mode VCSEL arrays with single-polarized outputs by using package-induced tensile strain. Opt. Lett. **45**, 4839–4842 (2020)
14. S. Ryoichiro, M. Hiroshi, F. Masayuki, N. Kazuki, J. Naoto, New wavelength tuning strategy for realizing VCSEL wafers with highly uniform wavelength. Proc. SPIE **11704**, 1170405 (2021)
15. Å. Haglund, J.S. Gustavsson, J. Vukušić, P. Modh, A. Larsson, Single fundamental-mode output power exceeding 6 mW from VCSELs with a shallow surface relief. IEEE Photon. Technol. Lett. **16**, 368–370 (2004)
16. A. Al-Samaneh, M. Bou Sanayeh, M.J. Miah, W. Schwarz, D. Wahl, A. Kern, R. Michalzik, Polarization-stable vertical-cavity surface-emitting lasers with inverted grating relief for use in microscale atomic clocks. Appl. Phys. Lett. **101**, 171104 (2012)
17. M. Rainer, *Fundamentals, technology and applications of vertical-cavity surface-emitting lasers*, vol. 166 (Springer Series in Optical Sciences, Ulm, 2013), p. 560
18. X. Zhang, Y. Zhang, J.W. Zhang, J. Zhang, C.Y. Zhong, Y.Q. Ning, S.H. Gu, L.J. Wang, 894 nm high temperature operatingvertical-cavity surface-emitting laser and its application in Cs chip-scale atomic-clock system. Acta Phys. Sinica **65**, 134204 (2016)

Publisher's Note Springer Nature remains neutral with regard to jurisdictional claims in published maps and institutional affiliations.